Published in final edited form as:
Bone. 2007 December ; 41(6): 928–936. doi:10.1016/j.bone.2007.07.022.

Callus mineralization and maturation are delayed during fracture healing in interleukin-6 knockout mice

Xu Yang, **Benjamin F. Ricciardi**, **Alexia Hernandez-Soria**, **Yuexian Shi**, **Nancy Pleshko Camacho**, and **Mathias P.G. Bostrom***
The Hospital for Special Surgery, 535 East 70th Street, New York, NY 10021, USA

Abstract

IL-6 is a pleiotropic cytokine involved in cell signaling in the musculoskeletal system, but its role in bone healing remains uncertain. The purpose of this study was to examine the role of IL-6 in fracture healing. Eight-week-old male C57BL/6 and IL-6 −/− mice were subjected to transverse, mid-diaphyseal osteotomies on the right femora. Sacrifice time points were 1, 2, 4, or 6 weeks post-fracture (*N*=14 per group). Callus tissue properties was analyzed by microcomputed tomography (micro-CT) and Fourier transform infrared imaging spectroscopy (FT-IRIS). Cartilage and collagen content, and osteoclast density were measured histologically. In intact unfractured bone, IL-6 −/− mice had reduced crystallinity, mineral/matrix ratio, tissue mineral density (TMD), and bone volume fraction (BVF) compared to wildtype mice. This suggests that there was an underlying deficit in baseline bone quality in IL-6 −/− mice. At 2 weeks post-fracture, the callus of IL-6 −/− mice had reduced crystallinity and mineral/matrix ratio. These changes were less evident at 4 weeks. At 2 weeks, the callus of the IL-6 −/− mice had an increased tissue mineral density (TMD), an increased cartilage and collagen content, and reduced osteoclast density compared to these parameters in wildtype mice. By 4 and 6 weeks, these parameters were no longer different between the two strains of mice. In conclusion, IL-6 −/− mice had delayed callus maturity, mineralization, and remodeling compared with the callus of the wildtype mice. These effects were transient indicating that the role of IL-6 appears to be most important in the early stages of fracture healing.

Keywords

Microcomputed tomography (micro-CT); Fourier transform infrared imaging spectroscopy (FT-IRIS); Interleukin 6; Cytokines; Fracture healing

Introduction

The fracture healing process consists of a complex cascade of events involving cells of the immune, hematopoietic, and musculoskeletal systems [1,2]. These interactions help reestablish mechanical stability in the injured tissue. Cytokines and growth factors such as PDGF, BMPs, and TNF-α play crucial roles in coordinating the interactions of these different cell populations in normal fracture healing [3–5]. Interleukin 6 (IL-6) is another cytokine that is important in cellular communication in the musculoskeletal system, but its role in the fracture healing response remains uncertain.

IL-6 is a pleiotropic cytokine which exists as a 184-amino acid peptide with a molecular weight of between 23 kDa and 32 kDa [6]. In bone, sources of IL-6 production include the osteoblast,

*Corresponding author. Fax: +1 212 472 3713. *E-mail address:* E-mail: bostromm@hss.edu (M.P.G. Bostrom).

mononuclear phagocytes, endothelial cells, chondrocytes, fibroblasts, and keratinocytes [7–9]. The release of IL-6 has been found to stimulate mesenchymal progenitor cells to differentiate towards the osteoblast lineage, and IL-6 binding to its receptor can induce the differentiation of peripheral blood monocytes into osteoclasts [9,10]. Receptors for IL-6 have been localized to the osteoclast cell membrane, and the combination of IL-6 and its soluble receptor can stimulate bone resorption activity by mature osteoclasts in vitro [11,12]. IL-6 also stimulates VEGF expression, suggesting that it plays a role in angiogenesis [13]. Since angiogenesis, and the differentiation and activity of osteoclasts and osteoblasts play major roles in fracture healing, IL-6 could be an important regulator of this process.

In order to examine the mineralized tissue properties in both fractured and unfractured bone, microcomputed tomography (micro-CT) and Fourier transform infrared imaging spectroscopy (FT-IRIS) were used. Micro-CT has recently been used to examine bone and mineral properties during the fracture healing response [14]. FT-IRIS enables infrared imaging of discrete regions of interest in histological sections of tissues at a resolution of 6.25 μm in combination with microscopic visualization of the samples [15]. While its use in analyzing the fracture healing response has been limited thus far, the ability of FT-IRIS to evaluate mineral quantity (relative mineral content) and quality (crystallinity) should be useful for studying the fracture healing process [15].

The purpose of our experiment is to investigate the role of IL-6 on callus mineralization, maturity, and remodeling during fracture healing in wild-type and IL-6 −/− mice. This is the first study that we are aware of that will address the specific role of IL-6 in the process of fracture healing in vivo.

Materials and methods

Production of fractures

All animal procedures were performed under an IACUC-approved protocol. Eight-week-old, male C57BL/6 control mice and strain-matched IL-6 −/− mice (Jackson Laboratory, Bar Harbor, ME) were subjected to closed, transverse, mid-diaphyseal osteotomies on the right femora that were stabilized with an intramedullary rod. Mice were sacrificed at 1 week, 2 weeks, 4 weeks, or 6 weeks post fracture. All animal procedures were approved by an Institutional Animal Care and Use Committee.

Micro-CT analysis

Mineralized tissue formation was assessed by microcomputed tomography (micro-CT). Right femora were harvested at 1, 2, 4, and 6 weeks post-fracture (*N*=9 per group). The specimens were placed in 70% ethanol and scanned by micro-CT using the MS-8 small animal scanner (GE Healthcare, Ontario, Canada) at a voltage of 80V and a current of 80 μA. A phantom containing an SB-2 bone analog (1.18 g/cm^3), water, and air samples was used for calibration in order to provide a standard of comparison between scans and to relate X-ray attenuation measurements to quantity of mineral in the tissue. Voxel size was isotropic and fixed at 46 μm. Images were reconstructed and thresholded to distinguish bone voxels.

Image analysis was performed using Microview v1.1 software (GE Healthcare). The volume of interest (VOI) was a fixed cylinder of 4 mm in diameter and 6 mm in height encompassing the entire volume of the fracture callus. This VOI was used for femurs collected 2, 4, and 6 weeks post-fracture (Fig. 1A). At 1 week, there was no radiographic evidence yet of fracture callus formation, and a cylinder of 4 mm in diameter and 3 mm in height encompassing the proximal part of the femur from the peak of the greater trochanter to the mid-diaphyseal region was used to provide a comparison of unfractured bone in the two strains of animals (Fig. 1B).

Within the VOI, the mineral mass divided by the volume (bone mineral density in milligrams per cubic centimeter) and fraction of bone within the volume (bone volume fraction) were calculated. For BVF measurements, bone was defined by a fixed threshold that was kept at a value of 400 Houndsfield units for all measurements.

The measured BMD was used to calculate the tissue mineral density (TMD), which is defined as the mass of mineralized tissue divided by the total volume of mineralized tissue. This differs from BMD because the unmineralized tissue and unoccupied space surrounding the callus and within the callus has been excluded from the measurement. We used this parameter to represent the density of the mineralized tissue in the callus. Tissue mineral density was defined as TMD=BMD/BVF.

Fourier transform infrared imaging spectroscopy (FT-IRIS)

Right femora were collected and embedded in PMMA at 2 and 4 weeks post-fracture (*N*=5 per group). For each femur, 2 μm longitudinal sections were cut through the center of the medullary canal using a Leica SM2500 microtome (Leica Microsystems, Bannockburn, IL). The sections were placed between two BaF_2 windows.

Transmission FT-IRIS data were acquired from histological sections at 8 cm^{-1} spectral resolution using a Spectrum Spotlight FT-IR Imaging system (Perkin-Elmer, Bucks, UK). This system is comprised of an FTIR spectrometer coupled with a light microscope and an 8 × 2 staggered linear array detector, and allows data collection over a user-defined rectangular region at 6.25 μm pixel resolution.

The first ROI analyzed was a rectangular box that extended from the cortical bone to the periphery of the callus. The center of the ROI was placed on the fracture line. A second rectangular ROI was placed inside of the cortical bone immediately proximal to the callus (Fig. 1C). FT-IRIS images were created based on the specific vibrational absorbances for each component of interest using ISys software v3.1 (Spectral Dimensions, Olney, MD). For each region, infrared vibrations of the mineral (biological apatite) and the matrix phases (mainly collagen) were monitored. The ratio of the area of the apatite phosphate absorbance (900–1200 cm^{-1}) to the area of the protein absorbance (1590–1720 cm^{-1}) was calculated. This ratio represents the relative amounts of mineral and matrix present (mineral/matrix ratio), an indicator of tissue density. Crystallinity of the mineral phase (indicative of relative maturity of the mineral) was calculated by the ratio of the intensity of the absorbance at 1030 cm^{-1} to that at 1020 cm^{-1}, a parameter previously shown to be related to the apatite crystal length in the *c*-axis direction [16].

Histology

After micro-CT scanning, tissue samples were decalcified in EDTA (*N*=9 per group) and embedded in paraffin. Six-micron-thick sections were cut longitudinally through the center of the medullary canal using a Reichert-Jung Biocut 2030 microtome (Leica Microsystems, Nussloch, Germany), placed onto Superfrost®/Plus microscope slides (Fischer Scientific, Pittsburgh, PA), and left overnight at 60 °C. Sections from 1, 2, 4, and 6 weeks post-fracture were stained routinely with Alcian Blue (Poly Scientific, Bay Shore, NY) and with modified Goldner's Trichrome staining [17].

Cathepsin K immunohistochemistry

Cathepsin K is an enzyme expressed by osteoclast cells. Six-micron-thick paraffin-embedded sections from the center of the callus were taken at 1, 2, 4, and 6 weeks post-fracture for cathepsin K immunohistochemistry. Sections were deparaffinized and incubated with anti-goat cathepsin K polyclonal antibody (C-16; Santa Cruz Biotechnology, Santa Cruz, CA) at room

temperature overnight. A Vectastain avidin–biotin–peroxidase complex (ABC) kit (Vector Laboratory, Burlingame, CA) was used with 3–3′ diaminobenzidine (Sigma-Aldrich) to visualize anti-cathepsin K positive cells. Anti-cathepsin K positive cells appeared with a brown cellular stain [18].

Proliferating cell nuclear antigen (PCNA) immunohistochemistry

Positive PCNA immunoreactivity is used as a marker of cell proliferation, and anti-PCNA positive cells appeared with a brown nuclear stain [19]. Six-micron-thick paraffin-embedded sections from the center of the callus were taken at 1, 2, 4, and 6 weeks post-fracture. These were deparaffinized and incubated with anti-mouse PCNA monoclonal antibody (PC-10; Santa Cruz Biotechnology) at room temperature overnight. Secondary antibodies and labeled streptavidin–biotin reagents (DAKO) were used with 3–3′ diaminobenzidine (10 mg in 15 mL of 1× PBS with 12 μL of hydrogen peroxide; Sigma-Aldrich) to visualize anti-PCNA positive cells.

Histomorphometry

Sections stained with Alcian Blue and Modified Goldner's Trichrome were visualized at ×1 magnification using a light microscope equipped with a digital imaging system (Nikon Microphot-FXA, Nikon, Melville, NY). Bioquant Nova software (Bioquant Image Analysis Corporation, Nashville, TN) was utilized for histomorphometric analysis. All measurements were performed in a blinded fashion. The region of interest (ROI) was defined as the area of the callus on both sides of the medullary canal excluding all cortical bone. This ROI was outlined manually for each specimen using the software.

Alcian Blue-positive proteoglycan appeared with a blue stain in the callus and was considered to be cartilage. Modified Goldner's Trichrome-positive collagen appeared with a green stain in the fracture callus. These stained areas were thresholded automatically by the software, and the total stained area within the ROI was measured. The result was expressed as the percentage of the total callus area. For all slides, two consecutive sections from the center of each fracture callus were analyzed, and these results were averaged.

For anti-cathepsin K stained slides, osteoclasts were considered to be anti-cathepsin K positive cells with at least three nuclei located adjacent to a bone surface. Regions of active callus resorption were located manually in the callus on one side of the medullary canal at ×20 magnification. One random field within these areas was visualized at ×40 magnification. The number of osteoclasts within this area was counted manually. This measurement was repeated for the callus on both sides of the medullary canal so that four fields were examined for each specimen. Two consecutive specimens from the center of the fracture callus were used for each animal giving a total of eight measurements per callus. Results were expressed as the average number of osteoclasts per mm^2.

For anti-PCNA stained slides, anti-PCNA positive cells immediately adjacent to regions of cartilage were considered to be chondroprogenitor cells. The cartilaginous region of the callus was visualized at ×20 magnification. For each measurement, the number of anti-PCNA-positive cells was counted in three random fields on the periphery of the cartilaginous zone of the callus. The total number of cells in the same field was then counted, and the percentage of anti-PCNA-positive cells per mm^2 was calculated. Three total fields were measured for each specimen, and two consecutive specimens from the center of the fracture callus were examined for each animal, giving a total of six measurements per animal. Cell proliferation within the cartilaginous region of the callus was expressed as the average percentage of anti-PCNA-positive cells per mm^2.

Statistics

Data were analyzed by two-way analysis of variance (ANOVA) by Sigma Stat software (SPSS Inc., Chicago, IL) using time post-fracture and genotype as parameters. A Bonferroni post-hoc test was used for pairwise comparisons between different treatment groups. Significance was defined at the $p<0.05$ level. All means are expressed±standard deviations.

Results

Intact bone

Micro-CT—In unfractured cortical bone, average TMD was significantly greater in the wildtype mice than in the IL-6 −/− mice (451.7±35.3 mg/cm^3 vs. 415.6±38.5 mg/cm^3 respectively; $p=0.029$) (Fig. 2A). In unfractured bone, BVF was greater in the region of interest in the wildtype mice compared to the IL-6 −/− mice, and this difference trended towards significance ($p=0.054$) (Fig. 2B).

FT-IRIS—Analysis of unfractured cortical bone by FT-IRIS analysis demonstrated an increased crystallinity, indicative of more mature mineral, in wildtype mice compared to IL-6 −/− mice at 2 weeks (1.124±0.026 vs. 1.066±0.0186 respectively; $p=0.009$) (Fig. 3A). There was an increased mineral/matrix ratio in cortical bone of wildtype mice compared to IL-6 −/− mice at 2 weeks that trended towards significance (5.78±1.047 vs. 4.68±0.91 respectively; $p=0.088$) and at 4 weeks (6.60±1.08 vs. 4.30±0.71 respectively; $p=0.007$) (Fig. 4A).

Callus formation and remodeling

Micro-CT—At 2 weeks, average TMD of the callus decreased in both strains of mice, and there was no longer any significant difference between the two strains (Fig. 2A). In addition, BVF of the callus area had peaked in the wildtype and the IL-6 −/− mice, and there was no significant difference between the two strains. This suggest that IL-6 −/− mice and the wildtype mice had similar volumes of bone at 2 weeks post-fracture, but the mineralized tissue in the callus of the IL-6 −/− mice had a greater density. At 4 weeks, TMD of the callus in both strains increased and the callus of the wildtype mice had a significantly greater TMD than the callus of the IL-6 −/− mice (490.7±30.5 mg/cm^3 vs. 450.1±27.3 mg/cm^3 respectively; $p=0.015$) (Fig. 2A). At 6 weeks, the callus of the wildtype mice continued to have a significantly greater TMD than the callus of the IL-6 −/− mice (505.0±30.6 mg/cm^3 vs. 433.3±40.1 mg/cm^3 respectively; $p<0.001$) (Fig. 2A).

FT-IRIS—At 2 weeks post-fracture, callus crystallinity was significantly greater in the wildtype mice compared with the IL-6 −/− mice (1.108±0.028 vs. 1.030±0.010 respectively; $p<0.001$) indicating that the wildtype callus had increased crystal maturity (Fig. 3B and Fig. 5). The increased callus crystallinity in the wildtype mice compared with the IL-6 −/− mice persisted at 4 weeks with a trend towards significance (1.093±0.036 vs. 1.0465±0.023 respectively; $p=0.051$). At 2 weeks post-fracture, the callus tissue of the wildtype mice had an increased mineral/matrix ratio compared to the IL-6 −/− mice that also trended towards significance (4.24±1.47 vs. 2.6±1.06 respectively; $p=0.082$) (Fig. 4B and Fig. 5). This difference was not present by 4 weeks.

Histology and immunohistochemistry

At 1 week, the percentage of cartilage in the callus was significantly greater in the IL-6 −/− mice compared to the wildtype mice (37.1±13.6% vs. 17.7±8.6% respectively; $p=0.002$) (Fig. 6A). At 2 weeks, the IL-6 −/− mice callus had a significantly greater cartilage percentage compared with the wildtype mice (19.3±12.4% vs. 10.4±6.2% respectively; $p=0.023$). There were no significant differences between wildtype and IL-6 −/− mice in the density of

proliferating cells in the callus at any time post-fracture. At 2 weeks, the callus of the IL-6 −/− mice had a significantly greater collagen percentage compared to the callus of the wildtype mice (41.7±7.4% vs. 22.8±5.6% respectively; $p<0.001$) (Fig. 6B). At 2 weeks, the callus of the wildtype mice had a significantly greater osteoclast density than the IL-6 −/− mice (30.0 ±6.8 osteoclasts/mm^2 vs. 23.9±3.07 osteoclasts/mm^2 respectively; $p=0.048$) (Fig. 7). At 4 weeks and 6 weeks, there was no longer any significant difference in cartilage content or osteoclast density between the two strains.

Discussion

Cell signaling molecules such as the inflammatory cytokines are expressed during fracture healing, and previous studies have shown that they are involved in the regulation of the repair process [1,20–25]. While the effects of many pro-inflammatory cytokines have been examined in fracture healing in vivo, no previous studies have attempted to isolate the role of IL-6 in this process.

In normal bone development, previous studies using wildtype mice have shown that mineral/matrix ratio of cortical bone tends to increase over time as the animals mature [26,27]. This suggests increased mineralization of cortical bone occurs normally during skeletal maturation. During endochondral ossification, which occurs in both the growth plate during development and in the fracture callus, the crystals that are initially formed during cartilage mineralization are poorly crystalline and contain areas of weakly organized regions; however, crystallinity proceeds to increase with age [28,29]. From our current study, it appears that IL-6 may be important in regulating bone maturation during development. We examined bone mineral properties in unfractured cortical bone in wildtype and IL-6 −/− mice, and the absence of IL-6 signaling resulted in a lower TMD, BVF, mineral/matrix ratio, and crystallinity of unfractured cortical bone. Both the decreased mineral/matrix ratio and TMD suggest that a decreased cortical bone density was present in IL-6 −/− mice. Crystallinity of cortical bone in IL-6 −/− mice was also decreased, suggesting that the absence of IL-6 signaling resulted in impaired crystal maturation [15]. Previous studies of IL-6 −/− mice have reported accelerated bone turnover and decreased cortical bone volume [30]. It is possible that an increased bone turnover could have contributed to decreased mineralization and crystal maturity during development in IL-6 −/− mice. The role of IL-6 in skeletal mineralization will have to be investigated further in future experiments.

In addition to its effects on bone development, IL-6 signaling appears to play an important role in the early stages of fracture healing. During the first 2 weeks of fracture healing, cartilage content of the callus was increased in the absence of IL-6 signaling. Previous studies have shown that IL-6 can suppress chondrocyte proliferation and decrease the differentiation of growth plate chondrocytes, although this role of IL-6 appears to be controversial [31,32]. There was no evidence of increased progenitor cell proliferation at 1 week in the IL-6 −/− callus, but it is possible that this effect on cell proliferation took place earlier than 1 week. IL-6 has also been shown to stimulate angiogenesis and cartilage matrix catabolism, and both processes are important in cartilage mineralization and turnover. IL-6 induces cartilage matrix catabolism through the expression of MMP-13, collagenase 3, and aggrecanase [33–35]. In vitro, IL-6 upregulates the expression of vascular endothelial growth factor in multiple cell lines [13]. The role of IL-6 in angiogenesis appears particularly relevant to fracture healing, and one study of skin wound healing in IL-6 −/− mice revealed impaired leukocyte infiltration and angiogenesis [36]. In addition, the release of IL-6 has been found to stimulate mesenchymal progenitor cells to differentiate towards the osteoblast lineage [9]. Vascular invasion, breakdown of the cartilage matrix, and osteoblast differentiation are crucial to callus mineralization and maturation, and the absence of IL-6 could delay these processes.

Similar to its effects during development, the absence of IL-6 signaling resulted in delayed mineralization and callus maturation in the first 2 weeks of fracture healing. TMD measured by micro-CT includes only mineralized tissue within the volume of interest in the measurement. In unfractured bone, the wildtype mice had an increased TMD compared with the IL-6 −/− mice. TMD decreased in both mouse strains at 2 weeks post-fracture compared to cortical bone alone because of the formation of less mineralized callus tissue in the volume of interest. However, the TMD of the cortical bone plus the fracture callus were similar between wildtype and IL-6 −/− mice at 2 weeks, suggesting that the IL-6 −/− mice had an increased density of the mineralized tissue in the callus compared with the wildtype at 2 weeks. The TMD measurement only examines mineralized tissue in the callus. In order to examine both mineralized callus and unmineralized matrix, the mineral/matrix ratio was calculated. This measurement represents the total tissue density of the callus, including unmineralized tissue. Mineral/matrix ratio was increased in the callus of the wildtype at 2 weeks relative to the callus of the IL-6 −/−. This difference was no longer present at 4 weeks, suggesting that mineralization was merely delayed in the IL-6 −/−. The wildtype callus also had an increased crystallinity relative to the IL-6 −/− callus suggesting that the wildtype callus had more mature mineral at 2 weeks. This difference was less marked at 4 weeks, further suggesting delayed callus maturation and mineralization in the absence of IL-6.

In addition to its potential role in cartilage matrix degradation and angiogenesis, IL-6 appears to be important in osteoclastogenesis in the callus. In our study, the absence of IL-6 signaling reduced the average osteoclast density in the callus of the IL-6 −/− mice at 2 weeks post-fracture. IL-6 signaling has been found to increase the differentiation of osteoclast precursor cells into mature osteoclasts in vitro [10,37–39]. Osteoclast resorption of woven bone is a necessary step in callus remodeling and maturation. Both of these processes were delayed in the absence of IL-6, and it was possible that the reduced number of osteoclasts contributed to these findings.

The absence of IL-6 signaling in our experiment had the greatest effect on the repair process in the early stages of fracture healing, a finding supported by in vivo and clinical studies. IL-6 expression has been found to peak at day 3 of the fracture healing process in a rat femoral fracture model [1]. This is in contrast to TNF-α and IL-1, which were expressed most strongly later in the healing process [1]. Additionally, clinical studies have found that serum IL-6 levels are elevated immediately after long-bone fracture [40]. The potential roles of IL-6 in contributing to angiogenesis and osteoclastogenesis could explain the importance of IL-6 signaling in early stages of fracture healing.

At 4 and 6 weeks post-fracture, the absence of IL-6 signaling did not appear to affect callus mineralization, cartilage remodeling, or osteoclastogenesis. In the later stages of fracture healing, other cytokines present in the fracture callus could compensate for any effect that the absence of IL-6 has on cartilage and bone remodeling. Tumor necrosis factor alpha (TNF-α) stimulates endochondral callus remodeling through its effects on angiogenesis and metallomatrix protease expression [22,41]. In addition, TNF-α and IL-1 played important roles in type I collagen remodeling at later stages of fracture healing [20]. From these past studies, it appears that other cytokines such as TNF-α could compensate for the absence of IL-6 later in the fracture healing process, as there appears to be considerable redundancy in cytokine stimulation of osteoclastogenesis, angiogenesis, and the endochondral tissue remodeling.

A potential limitation of this study was the relatively small sample size in some groups in the FT-IRIS analysis. Differences in crystallinity and mineral/matrix ratio only trended towards significance between the wildtype and IL-6 −/− mice at certain time points. A power analysis had been performed prior to the current study based on data from previous studies that have been done using FT-IRIS in mouse models [26,42,43]. These studies used similar sample sizes

when assessing bone mineral properties using FT-IRIS, however, none of these previous studies were fracture healing studies. The experimental variation was greater than expected in the FT-IRIS analysis in this study possibly due to variability in the fracture healing process. A decreased power in a study can increase the risk of beta error. Consequently, it is possible that some of the other differences in FT-IRIS properties may not have reached statistical significance due to inadequate sample size in each group. The sample size used in the histologic analysis in this study was similar to previous studies of fracture healing in mice, and appeared to be adequate to detect differences in callus properties between the two strains of mice [44, 45]. The high statistical significance of the cartilage content and collagen content measurements at 1 week and 2 weeks respectively suggest that these parameters appear to be primary effects of IL-6 signaling in fracture healing. The borderline statistical significance of the osteoclast data may be a reflection of the fact that other cytokines such as TNF-alpha most likely are more important regulators of osteoclastogenesis during fracture healing, hence, IL-6 has a more modest effect.

In conclusion, the fracture callus of IL-6 −/− mice had decreased total callus tissue density and less mature mineral at 2 weeks post-fracture. This was accompanied histologically by increased cartilage and collagen content, and a decreased osteoclast density. These differences suggest delayed callus mineralization and remodeling in the absence of IL-6. These effects were only transient, however, as callus maturation and remodeling did occur by 4 weeks post-fracture. IL-6 signaling therefore appeared to play a role in the early stages of fracture healing, but its role diminished over time.

Acknowledgments

Support for this project was provided by AR48337 (to NPC) and the Oxnard Foundation (to MPGB). This study utilized the facilities of the HSS Core Center for Musculoskeletal Integrity, supported by NIH AR46121.

References

1. Einhorn TA, Majeska RJ, Rush EB, Levine PM, Horowitz MC. The expression of cytokine activity by fracture callus. J Bone Miner Res 1995;10(8):1272–1281. [PubMed: 8585432]
2. Einhorn TA. The cell and molecular biology of fracture healing. Clin Orthop Relat Res 1998;355S:S7–S21. [PubMed: 9917622]
3. Andrew JG, Hoyland JA, Freemont AJ, Marsh DR. Platelet-derived growth factor expression in normally healing human fractures. Bone 1995;16(4):455–460. [PubMed: 7605706]
4. Gerstenfeld LC, Cho TJ, Kon T, Aizawa T, Cruceta J, Graves BD, Einhorn TA. Impaired intramembranous bone formation during bone repair in the absence of tumor necrosis factor-alpha signaling. Cells Tissues Organs 2001;169(3):285–294. [PubMed: 11455125]
5. Lieberman JR, Daluiski A, Einhorn TA. The role of growth factors in the repair of bone. J Bone Jt Surg 2002;84-A:1032–1044.
6. Wong PKK, Campbell IK, Egan PJ, Ernst M, Wicks IP. The role of the interleukin-6 family of cytokines in inflammatory arthritis and bone turnover. Arthritis Rheum 2003;48:1177–1189. [PubMed: 12746890]
7. Littlewood AJ, Russell J, Harvey GR, Hughes DE, Russell RG, Gowen M. The modulation of the expression of IL-6 and its receptor in human osteoblasts in vitro. Endocrinology 1991;129(3):1513–1520. [PubMed: 1714833]
8. Haynes DR, Hay SJ, Rogers SD, Ohta S, Howie DW, Graves SE. Regulation of bone cells by particle-activated mononuclear phagocytes. J Bone Jt Surg [Br] 1997;79-B:988–994.
9. Heymann D, Rousselle AV. Gp130 cytokine family and bone cells. Cytokine 2000;12(10):1455–1468. [PubMed: 11023660]
10. Kudo O, Sabokbar A, Pocock A, Itonaga I, Fujikawa Y, Athanasou NA. Interleukin-6 and interleukin-11 support human osteoclast formation by a RANKL-independent mechanism. Bone 2003 Jan;32(1):1–7. [PubMed: 12584029]

11. Adebanjo OA, Moonga BS, Yamate T, Sun L, Minkin C, Abe E, et al. Mode of action of interleukin-6 on mature osteoclasts. Novel interactions with extracellular Ca2+ sensing in the regulation of osteoclastic bone resorption. J Cell Biol 1998 Sep 7;142(5):1347–1356. [PubMed: 9732294]
12. Palmqvist P, Persson E, Conaway HH, Lerner UH. IL-6, leukemia inhibitory factor, and oncostatin M stimulate bone resorption and regulate the expression of receptor activator of NF-kappa B ligand, osteoprotegerin, and receptor activator of NF-kappa B in mouse calvariae. J Immunol 2002;169:3353–3362. [PubMed: 12218157]
13. Cohen T, Nahari D, Cerem LW, Neufeld G, Levi BZ. Interleukin 6 induces the expression of vascular endothelial growth factor. J Biol Chem 1996;271:736–741. [PubMed: 8557680]
14. Gardner MJ, van der Meulen MC, Demetrakopoulos D, Wright TM, Myers ER, Bostrom MP. In vivo cyclic axial compression affects bone healing in the mouse tibia. J Orthop Res 2006;24(8):1679–1686. [PubMed: 16788988]
15. Camacho NP, Carroll P, Raggio CL. Fourier transform infrared imaging spectroscopy (FT-IRIS) of mineralization in bisphosphonate-treated oim/oim mice. Calcif Tissue Int 2003;72(5):604–609. [PubMed: 12574874]
16. Gadaleta SJ, Paschalis EP, Betts F, Mendelsohn R, Boskey AL. Fourier transform infrared spectroscopy of the solution-mediated conversion of amorphous calcium phosphate to hydroxyapatite: new correlations between X-ray diffraction and infrared data. Calcif Tissue Int 1996;58:9–16. [PubMed: 8825233]
17. Goldner J. A modification of the Masson trichrome technique for routine laboratory purposes. Am J Pathol 1938;14:237–243.
18. Motyckova G, Fisher DE. Pycnodysostosis: role and regulation of cathepsin K in osteoclast function and human disease. Curr Mol Med 2002;2(5):407–421. [PubMed: 12125807]
19. Takasaki Y, Deng JS, Tan EM. A nuclear antigen associated with cell proliferation and blast transformation. J Exp Med 1981;154:1899–1909. [PubMed: 6172535]
20. Kon T, Cho T, Aizawa T, Yamazaki M, Nooh N, Graves D, Gerstenfeld LC, Einhorn TA. Expression of osteoprotegerin, receptor of activator of NF-kB ligand and related proinflammatory cytokines during fracture healing. J Bone Miner Res 2001;16(6):1004–1014. [PubMed: 11393777]
21. Flick LM, Weaver JM, Ulrich-Vinther M, Abuzzahab F, Zhang X, Dougall WC, et al. Effects of receptor activator of NFkB (RANK) signaling blockade on fracture healing. J Orthop Res 2003;21:676–684. [PubMed: 12798068]
22. Lehmann W, Edgar CM, Wang K, Cho TJ, Barnes GL, Kakar S, et al. Tumor necrosis factor alpha (TNF-alpha) coordinately regulates the expression of specific matrix metalloproteinases (MMPS) and angiogenic factors during fracture healing. Bone 2005;36:300–310. [PubMed: 15780956]
23. Kloen P, Di Paola M, Borens O, Richmond J, Perino G, Helfet DL, Goumans MJ. BMP signaling components are expressed in human fracture callus. Bone 2003;33:362–371. [PubMed: 13678778]
24. Street J, Bao M, deGuzman L, Bunting S, Peale FV Jr, Ferrara N, et al. Vascular endothelial growth factor stimulates bone repair by promoting angiogenesis and bone turnover. Proc Natl Acad Sci U S A 2002;99(15):9656–9661. [PubMed: 12118119]
25. Cho TJ, Gerstenfeld LC, Einhorn TA. Differential temporal expression of members of the transforming growth factor beta superfamily during murine fracture healing. J Bone Miner Res 2002;17:513–520. [PubMed: 11874242]
26. Ling Y, Rios HF, Myers ER, Lu Y, Feng JQ, Boskey AL. DMP1 depletion decreases bone mineralization in vivo: an FTIR imaging analysis. J Bone Miner Res 2005 Dec;20(12):2169–2177. [PubMed: 16294270]
27. Boskey AL, Gadaleta S, Gundberg C, Doty SB, Ducy P, Karsenty G. Fourier transform infrared microspectroscopic analysis of bones of osteocalcin-deficient mice provides insight into the function of osteocalcin. Bone 1998 Sep;23(3):187–196. [PubMed: 9737340]
28. Magne D, Bluteau G, Faucheux C, Palmer G, Vignes-Colombeix C, Pilet P, et al. Phosphate is a specific signal for ATDC5 chondrocyte maturation and apoptosis-associated mineralization: possible implication of apoptosis in the regulation of endochondral ossification. J Bone Miner Res 2003;18(8):1430–1442. [PubMed: 12929932]
29. Matsushima N, Hikichi K. Age changes in the crystallinity of bone mineral and in the disorder of its crystal. Biochim Biophys Acta 1989 Aug 18;992(2):155–159. [PubMed: 2758062]

30. Poli V, Balena R, Fattori E, Markatos A, Tamamoto M, Tanaka H, et al. Interleukin-6 deficient mice are protected from bone loss caused by estrogen depletion. EMBO J 1994;13(5):1189–1196. [PubMed: 8131749]

31. Jikko A, Wakisaka T, Iwamoto M, Hiranuma H, Kato Y, Maeda T, et al. Effects of interleukin-6 on proliferation and proteoglycan metabolism in articular chondrocyte cultures. Cell Biol Int 1998;22:615–621. [PubMed: 10452831]

32. Kitamura H, Kawata H, Takahashi F, Higuchi Y, Furuichi T, Ohkawa H. Bone marrow neutrophilia and suppressed bone turnover in human interleukin-6 transgenic mice. Am J Pathol 1995;147:1682–1691. [PubMed: 7495293]

33. Solis-Herruzo JA, Rippe RA, Schrum LW, de La Torre P, Garcia I, Jeffrey JJ. Interleukin-6 increases rat metalloproteinase-13 gene expression through stimulation of activator protein 1 transcription factor in cultured fibroblasts. J Biol Chem 1999;274:30919–30926. [PubMed: 10521486]

34. Franchimont N, Rydziel S, Delany AM, Canalis E. Interleukin-6 and its soluble receptor cause a marked induction of collagenase 3 expression in rat osteoblast cultures. J Biol Chem 1997;272:12144–12150. [PubMed: 9115285]

35. Flannery CR, Little CB, Hughes CE, Curtis CL, Caterson B, Jones SA. IL-6 and its soluble receptor augment aggrecanase-mediated proteoglycan catabolism in articular cartilage. Matrix Biol 2000;19:549–553. [PubMed: 11068209]

36. Lin ZQ, Kondo T, Ishida Y, Takayasu T, Mukaida N. Essential involvement of IL-6 in the skin wound-healing process as evidenced by delayed wound healing in IL-6-deficient mice. J Leukoc Biol 2003;73(6):713–721. [PubMed: 12773503]

37. Neale SD, Sabokbar A, Howie DW, Murray DW, Athanasou NA. Macrophage colony-stimulating factor and interleukin-6 release by periprosthetic cells stimulates osteoclast formation and bone resorption. J Orthop Res 1999;17:686–694. [PubMed: 10569477]

38. Tamura T, Udagawa N, Takahashi N, Miyaura C, Tanaka S, Yamada Y, et al. Soluble interleukin-6 receptor triggers osteoclast formation by interleukin 6. Proc Natl Acad Aci U S A 1993;90:11924–11928.

39. Gorny G, Shaw A, Oursler MJ. IL-6, LIF, and TNF-alpha regulation of GM-CSF inhibition of osteoclastogenesis in vitro. Exp Cell Res 2004;294:149–158. [PubMed: 14980510]

40. Strecker W, Gebhard F, Rager J, Bruckner UB, Steinbach G, Kinzl L. Early biochemical characterization of soft-tissue trauma and fracture trauma. J Trauma 1999;47(2):358–364. [PubMed: 10452474]

41. Gerstenfeld LC, Cho TJ, Kon T, Aizawa T, Tsay A, Fitch J, et al. Impaired fracture healing in the absence of TNF-alpha signaling: the role of TNF-alpha in endochondral cartilage resorption. J Bone Miner Res 2003;8(9):1584–1592. [PubMed: 12968667]

42. Atti E, Gomez S, Wahl SM, Mendelsohn R, Paschalis E, Boskey AL. Effects of transforming growth factor-beta deficiency on bone development: a Fourier transform-infrared imaging analysis. Bone 2002 Dec;31(6):675–684. [PubMed: 12531561]

43. Boskey AL, Moore DJ, Amling M, Canalis E, Delany AM. Infrared analysis of the mineral and matrix in bones of osteonectin-null mice and their wildtype controls. J Bone Miner Res 2003 Jun;18(6): 1005–1011. [PubMed: 12817752]

44. Maes C, Coenegrachts L, Stockmans I, Daci E, Luttun A, Petryk A, et al. Placental growth factor mediates mesenchymal cell development, cartilage turnover, and bone remodeling during fracture repair. J Clin Invest 2006 May;116(5):1230–1242. [PubMed: 16614757]

45. Kayal RA, Tsatsas D, Bauer MA, Allen B, Al-Sebaei MO, Kakar S, et al. Diminished bone formation during diabetic fracture healing is related to the premature resorption of cartilage associated with increased osteoclast activity. J Bone Miner Res 2007 Apr;22(4):560–568. [PubMed: 17243865]

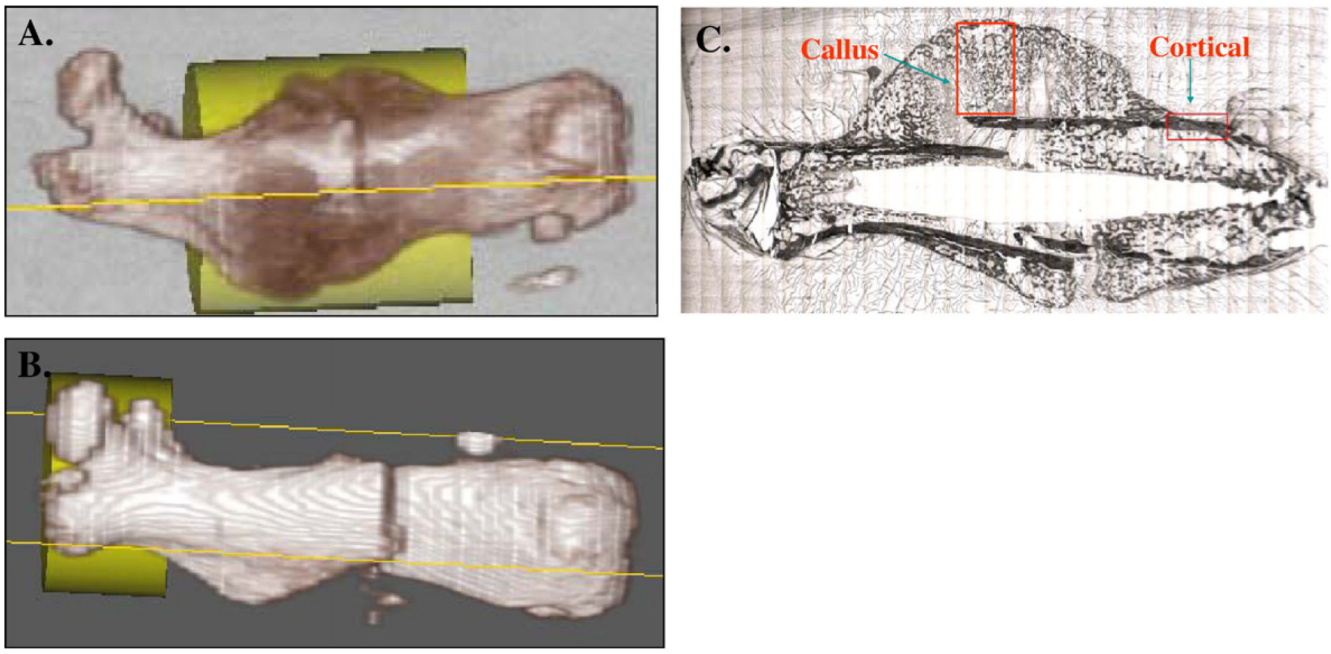

Fig. 1.

For micro-CT analysis at 2, 4, and 6 weeks post-fracture (A), the VOI was defined by a cylinder of 4 mm in diameter and 6 mm in height encompassing the diaphyseal portion of the femur which included the fracture callus. At 1 week post fracture (B), the VOI utilized was a cylinder of 4 mm in diameter and 3 mm in height encompassing the proximal part of the femur from the peak of the greater trochanter to the mid-diaphyseal region to provide a comparison of unfractured bone. For FT-IRIS analysis (C), the first ROI analyzed was a rectangular box that encompassed the cortical bone immediately proximal to the callus. A second rectangular ROI was placed inside of the callus excluding all cortical bone.

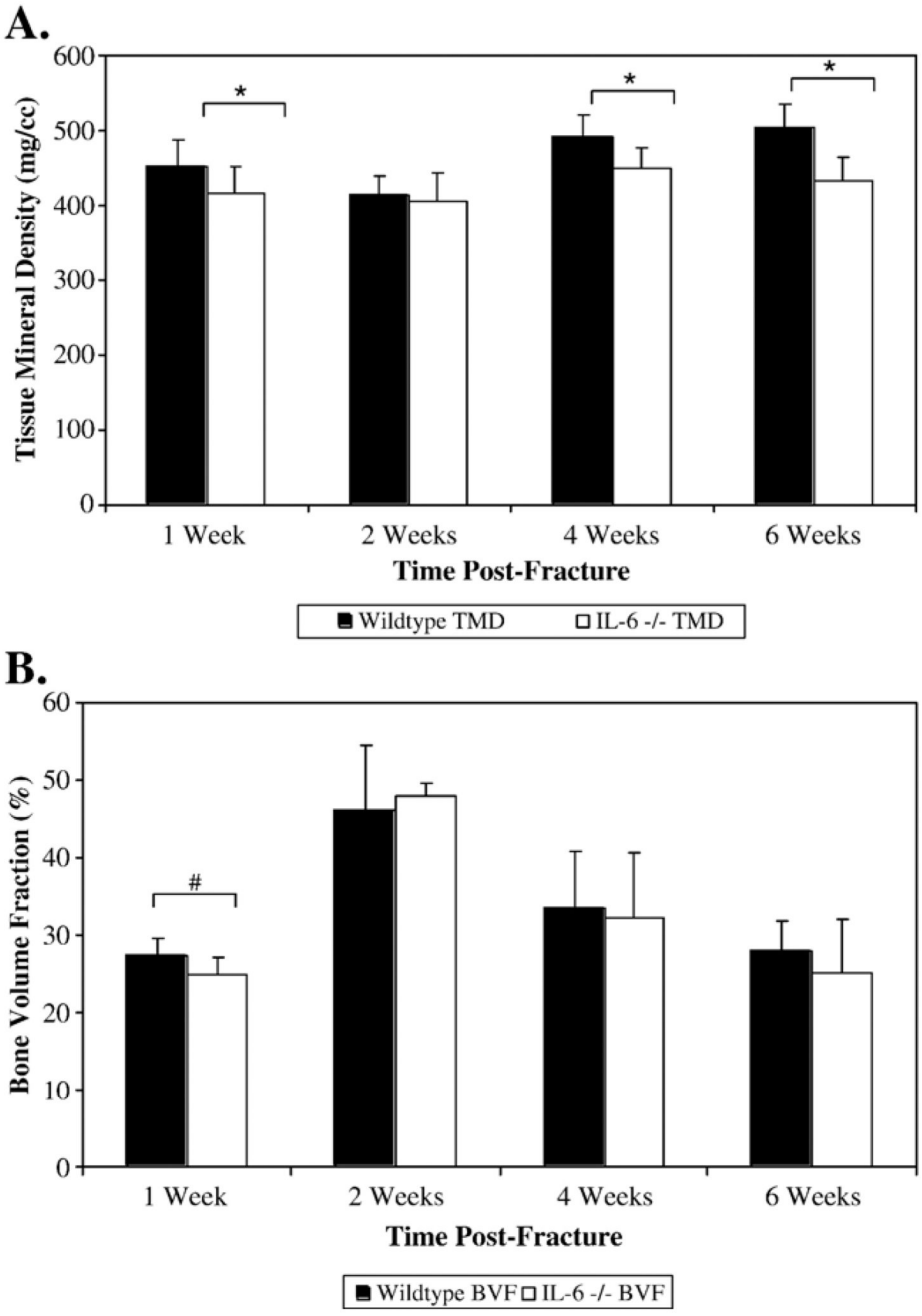

Fig. 2.

TMD (mg/cm^3) (A) and BVF (%) (B) were used to examine the density and quantity, respectively, of the mineralized callus tissue at 2, 4, and 6 weeks post-fracture. At 1 week, the TMD and BVF of unfractured bone was measured for the two strains of mice. * Denotes significance at $p<0.05$. # Denotes trend towards significance ($p=0.054$).

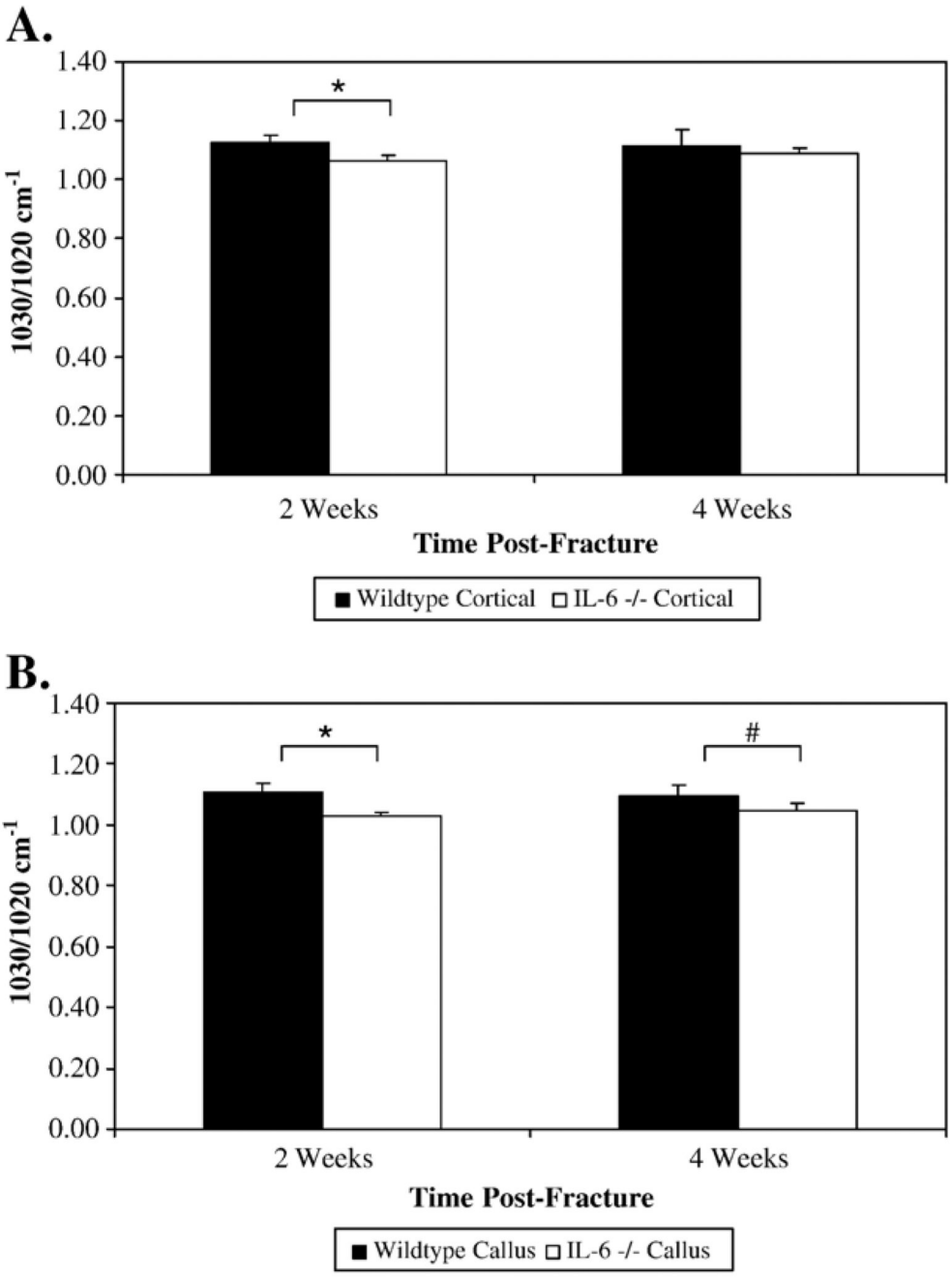

Fig. 3.

Crystallinity of cortical (A) and callus tissue (B) was measured in wildtype and IL-6 −/− bone. Crystallinity of the mineral phase was calculated by the ratio of the intensity of the absorbance at 1030 cm^{-1} to that at 1020 cm^{-1}, a parameter previously shown to be related to crystal size. * Denotes significance at the $p<0.05$ level. # Denotes trend towards significance ($p=0.051$).

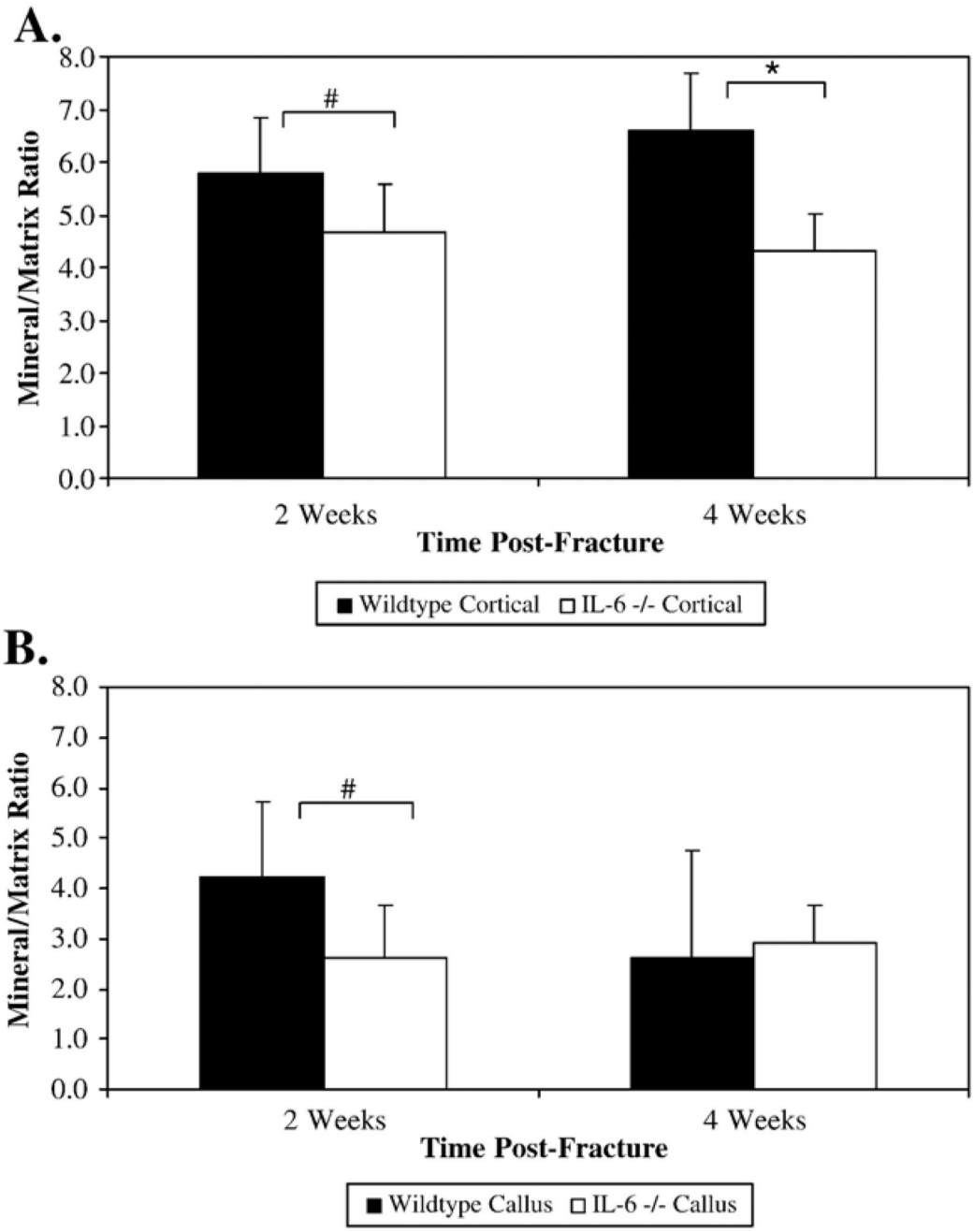

Fig. 4.

Mineral/matrix ratios were calculated from cortical (A) and callus (B) tissue of wildtype and IL-6 −/− mice. The ratio of the area of the apatite phosphate absorbance (900–1200 cm^{-1}) to the area of the protein absorbance (1590–1720 cm^{-1}) represents the relative amounts of mineral and matrix present, a parameter similar to tissue density. * Denotes significance at the $p<0.05$ level. # Denotes trending towards significance ($p=0.088$ and 0.082 respectively).

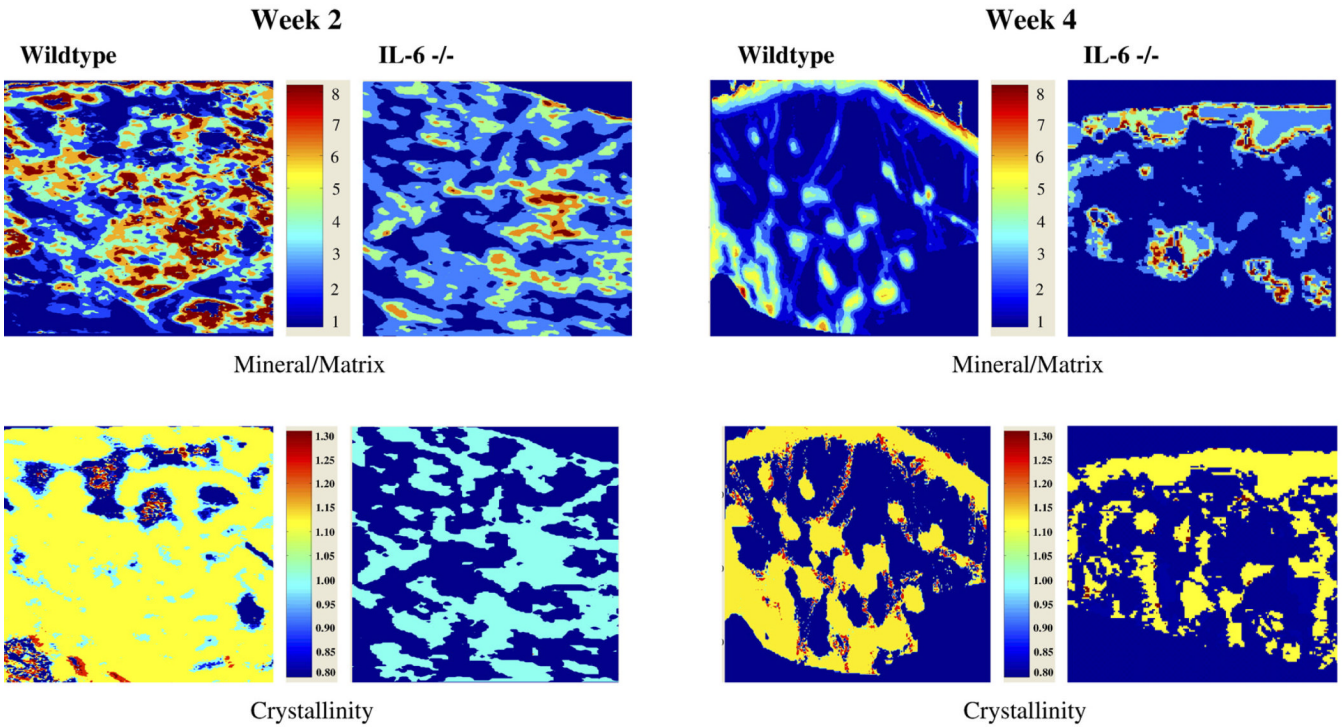

Fig. 5.
FT-IRIS images showing the crystallinity and mineral/matrix ratio of callus tissue at 2 and 4 weeks post-fracture in wildtype and IL-6 −/− mice.

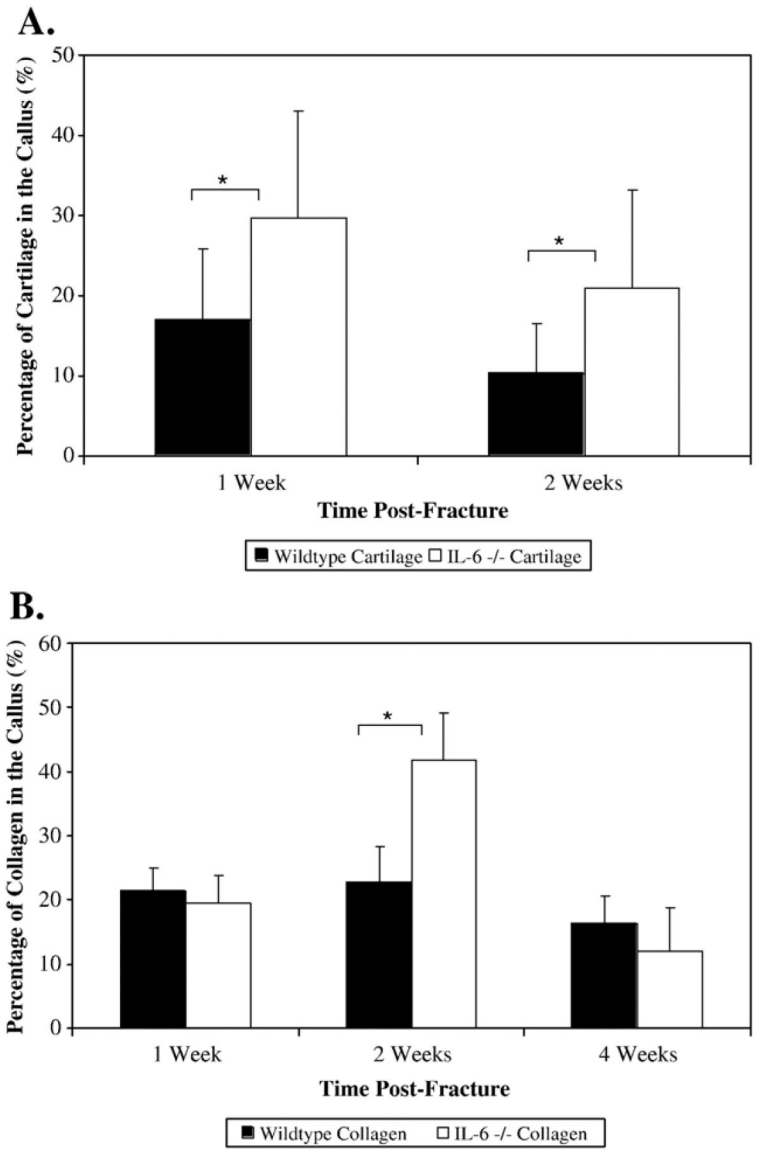

Fig. 6.

The percentage of cartilage (A) and collagen (B) in the fracture callus was measured using Alcian Blue and modified Goldner's Trichrome stained slides, respectively, collected from femurs at 1, 2, 4, and 6 weeks post-fracture. Results for cartilage percentage are shown only for 1 and 2 weeks post-fracture, as no cartilage remained after that time point. * Denotes significance at the $p<0.05$ level.

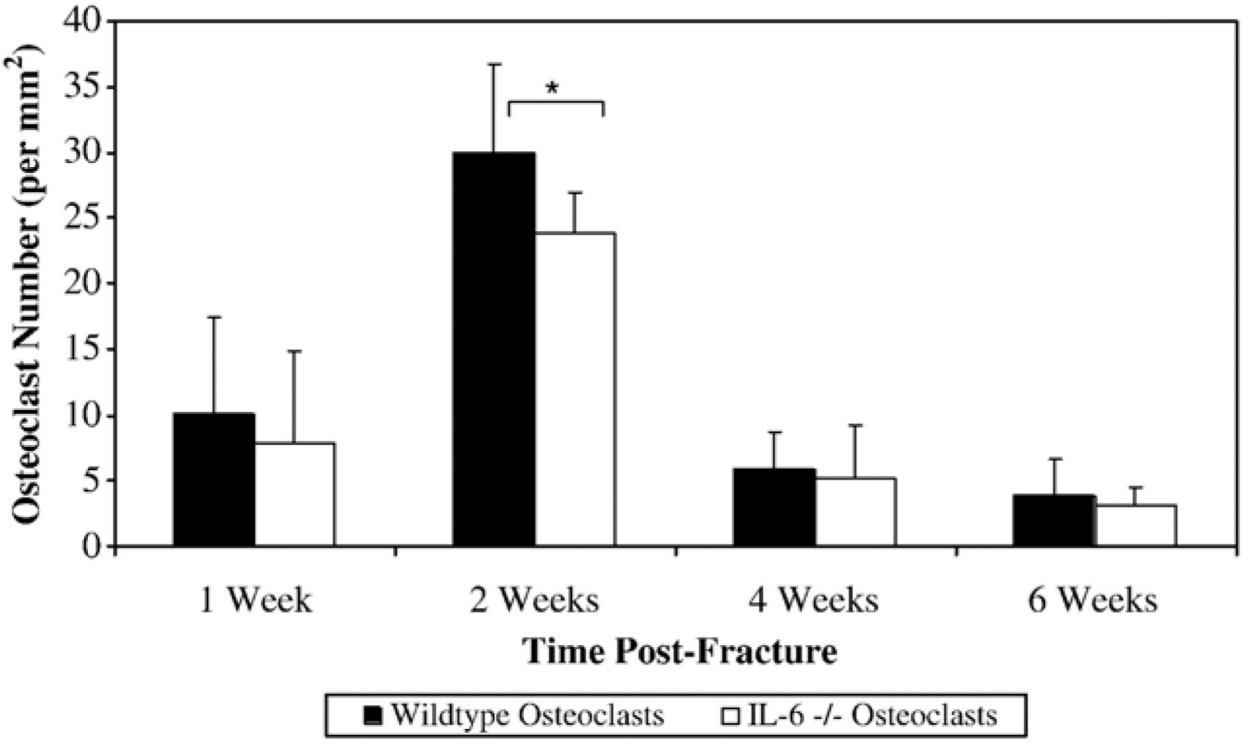

Fig. 7.

The osteoclast density within the fracture callus was measured by anti-cathepsin K staining. The number of multinucleated, anti-cathepsin K positive cells were counted in the fracture callus of both strains of animals at 1, 2, 4, and 6 weeks post-fracture. The results are expressed as the number of anti-cathepsin K positive osteoclasts per mm^2 area of the callus. * Denotes significance at the $p<0.05$ level.